International Journal of Heat and Mass Transfer 97 (2016) 589–595

Contents lists available at ScienceDirect

International Journal of Heat and Mass Transfer

journal homepage: www.elsevier.com/locate/ijhmt

Technical Note

Thermographic particle velocimetry (TPV) for simultaneous interfacial temperature and velocity measurements

Alexandros Charogiannis, Ivan Zadrazil, Christos N. Markides *

Clean Energy Processes (CEP) Laboratory, Department of Chemical Engineering, Imperial College London, London SW7 2AZ, United Kingdom

ARTICLE INFO

Article history:
Received 6 January 2016
Received in revised form 18 February 2016
Accepted 18 February 2016

Keywords:
Infrared thermography
Particle image velocimetry
Particle tracking velocimetry
Film flows
Interfacial temperature
Interfacial velocity

ABSTRACT

We present an experimental technique, that we refer to as 'thermographic particle velocimetry' (TPV), which is capable of the simultaneous measurement of two-dimensional (2-D) surface temperature and velocity at the interface of multiphase flows. The development of the technique has been motivated by the need to study gravity-driven liquid-film flows over inclined heated substrates, however, the same measurement principle can be applied for the recovery of 2-D temperature- and velocity-field information at the interface of any flow with a sufficient density gradient between two fluid phases. The proposed technique relies on a single infrared (IR) imager and is based on the employment of highly reflective (here, silver-coated) particles which, when suspended near or at the interface, can be distinguished from the surrounding fluid domain due to their different emissivity. Image processing steps used to recover the temperature and velocity distributions include the decomposition of each original raw IR image into separate thermal and particle images, the application of perspective distortion corrections and spatial calibration, and finally the implementation of standard particle velocimetry algorithms. This procedure is demonstrated by application of the technique to a heated and stirred flow in an open container. In addition, two validation experiments are presented, one dedicated to the measurement of interfacial temperature and one to the measurement of interfacial velocity. The deviations between the results generated from TPV and those from accompanying conventional techniques do not exceed the errors associated with the latter.

Liquid-film flows are a class of convectively unstable open-flow systems that can exhibit a rich variety of interfacial phenomena, complex wave patterns and dynamics [1]. Since the pioneering work of the father-son team of the Kapitza family [2,3], many theoretical [4,5], numerical [6,7] and experimental [8,9] efforts have been devoted to the understanding of the physical processes underlying these flows. Beyond the great fundamental interest in these flow systems, ongoing efforts have also been motivated by a strong desire to harness the high heat and mass transfer capabilities of thin-film flows in a wide range of engineering and industrial applications, including cooling schemes used in electronic and mechanical systems, heat exchangers, film condensers, evaporators, reactors, and many others.

Under non-isothermal conditions, the interfacial topology of liquid films is strongly influenced by Marangoni stresses induced by (temperature-related) surface tension gradients. The latter result from temperature non-uniformities over the interface and are responsible for destabilizing the flow and triggering several well-studied phenomena, such as film contraction, rivulet formation and film rupture.

Many recent experimental studies aiming to investigate heated-film flows have relied on the application of optical diagnostics in the search for increasing insight into these flows and the provision of highly detailed spatiotemporal information on their characteristics. A particularly popular optical technique is infrared (IR) thermography [10,11], which allows for temperature measurements to be performed over an extended, 2-D spatial domain with very high sensitivity (often around 20 mK) and accuracy (often better than 0.5 °C), at relatively high repetition-rates (of the order of 100 Hz). Furthermore, some of the commonly employed liquids in interfacial flow investigations, such as water and glycerol, are opaque over broad IR spectral bands, allowing for temperature measurements that are intergraded over extremely shallow optical depths (of the order of a few 10 s of μm). At this point, it is essential to acknowledge the work of Ito, Masunaga and Baba [12], and Kabov, Marchuk and Chupin [13], who contributed some of the

* Corresponding author at: Clean Energy Processes (CEP) Laboratory, Department of Chemical Engineering, Imperial College London, South Kensington Campus, London SW7 2AZ, United Kingdom. Tel.: +44 (0)20 759 41601.

E-mail addresses: ac1005@ic.ac.uk (A. Charogiannis), i.zadrazil06@imperial.ac.uk (I. Zadrazil), c.markides@imperial.ac.uk (C.N. Markides).

http://dx.doi.org/10.1016/j.ijheatmasstransfer.2016.02.050
0017-9310/

first experimental studies employing IR thermography in the investigation of falling-film flows. In the first case, the authors determined the temperature distribution on the gas–liquid interface of a thin-liquid film falling down a vertical tube, and linked the appearance of hot-spots to film-thinning and rupture. In the second, the interfacial temperature distributions of thin films flowing over a localised heater were measured as a function of the flow Reynolds number (*Re*) and the heat flux into the liquid, allowing the investigators to characterize, in great detail, the formation of standing waves due to the onset of the thermocapillary instability.

Comprehensive experimental investigations focusing on the effect of thermocapillary forces on wave topology in response to uniform [14], as well as localized heating [15–17], have been carried out at the Institute of Thermophysics of the Siberian Branch of the Russian Academy of Sciences. By employing IR thermography, the investigators have made several significant contributions, elucidating the link between the applied heat flux and the formation and spatiotemporal evolution of film regions dominated by thermal rivulets. In addition, Z.-B. Zhang and his co-workers [18–20] have published several studies based on thermal imaging, concentrating on film contraction/expansion as a function of both flow and heating parameters. Finally, the interaction between thermocapillary forces and the hydrodynamics of regular (solitary) wave patterns have been thoroughly investigated at the Institute of Heat and Mass Transfer of Aachen University [21,22]. IR thermography was employed alongside a film-height measurement technique in order to ascertain the role of the Marangoni effect. It should be noted that the publications cited here are by no means exhaustive, but rather only indicative of the number of relevant studies carried out by employing IR thermography in heated falling-film flows.

In this short communication we propose an alternative approach to the use of basic IR imaging for the study of heated falling-films. Building upon our recent work on unsteady and conjugate heat transfer in thin liquid-films flowing over a heated planar substrate under the action of gravity [23,24,11], we seek here to deepen our understanding of the phenomenology of rivulet formation in these flows by simultaneously conducting thermography and velocimetry measurements at the air–liquid interface. Kabov and co-workers [25] had previously tracked the fluid motion at the interface of an ethyl alcohol/water film subjected to localized heating by blowing Aluminium particles onto the interface, and recording the light reflected from particle clusters using a high-speed camera. Here, we propose instead the use of reflective (in the IR) particles and IR imaging alone in order to simultaneously recover the respective temperature and velocity fields. The applicability of the technique extends to many other multiphase/interfacial flows, where advanced detailed measurements are performed with the use of lasers [26–29].

In more detail, the proposed experimental technique is based on the employment of highly reflective, silver-coated particles, which when suspended near or at the air–liquid interface, are imaged as highly localized thermal radiation peaks or troughs. The thermal radiation collected by the IR camera, I_{meas}, when the latter is positioned over the liquid interface follows the relation given in Eq. (1):

$$I_{meas} = \epsilon I_{li} + (1-\epsilon) I_{bg}, \tag{1}$$

where ϵ stands for the emissivity of the liquid phase below the free surface, I_{li} for the thermal radiation emitted by the liquid, and I_{bg} for the background radiation reflected by the liquid as a result of its reflectivity $\rho = 1-\epsilon$.

The emissivities of water and glycerol, the two liquids employed in our experiments, amount to ≈0.96 [30], which suggests that very little background radiation is collected under the presently discussed imaging conditions. Nevertheless, it should be noted that in our experiments the IR camera was set at an offset angle (approximately 20°) to the air–liquid interface in order to prevent it from capturing a reflected image of itself. In contrast to the emissivity of these liquids, the emissivity of silver, the material used for coating the glass hollow spheres we employed for velocimetry purposes, is below 0.1 even when oxidized [30]. Consequently, a particle suspended at the interface will reflect strongly any background radiation, and thus, the emissive power seen by the IR detector will be largely dictated by the background temperature. There are two ways by which such particles can be distinguished from the surrounding fluid when imaged using an IR detector: (i) if the flow temperature is lower than the background temperature the particles appear as local glare spots, or (ii) if the background temperature is lower than the flow temperature, they appear as localized dark spots. IR images representative of both scenarios are presented in Fig. 1. In the first case, in Fig. 1(a), the liquid temperature corresponds to approximately 10 °C, and in the second in Fig. 1(b), to 50 °C, while the room (background) temperature is around 25 °C in both cases.

The two images shown in Fig. 1 were generated using a cooled, mid-wave FLIR X6540sc camera (15 μm pitch, 640 pixel × 520 pixel detector), a 650 W IKA RCT magnetic stirrer with intergraded temperature control, and a borosilicate-glass Petri dish (Fig. 2(a)). The quoted thermal sensitivity of the camera amounts to ≈18 mK, and the maximum recording frequency to 126 Hz (at full resolution). A 25 mm, F/2 lens, which is transmissive over the range 2.5–5 μm, was installed on the camera, allowing for a maximum spatial (pixel) resolution of up to ≈100 μm per pixel. Deionized water was seeded with silver-coated glass hollow-spheres of average diameter 100 μm and 12% silver content by weight (density of 0.9 g/mL). It is noted that the particles were selected to be buoyant/neutral in order to allow for interfacial velocity measurements with only a modest seeding concentration.

This setup was also employed in developing the experimental methodology and processing steps used for treating raw thermal images, such as those presented in Fig. 1, in order to extract temperature and velocity information. These processing steps will be presented here, alongside sample images corresponding to intermediate results; the latter will be used to facilitate the presentation. Fig. 3(a) shows a raw thermal image of the liquid surface (similar to the one presented in Fig. 1(b)), with the particle-seeded water heated to approximately 70 °C and continuously stirred at 100 rpm. The camera was positioned at a distance of ≈20 cm from the interface and at an angle of ≈20° to a plane normal to the surface (Fig. 2(a)). The detector response was first corrected for spatial non-uniformity by placing a blackbody in front of the lens, and for background radiation by setting up a diffuse mirror (crumpled Aluminium foil) and measuring the temperature independently. The (water) surface emissivity was set to 0.96 in the FLIR image acquisition and processing software, Research IRMax 3.3, and the atmospheric transmission to 1. Finally, the recording frequency was set to 100 Hz and the image integration time to 843 μs.

In order to correct raw thermal images for perspective distortions (the camera axis is set at an angle to the liquid free-surface, as stated above), a thermal target image of known spatial coordinates must be recorded. Towards this end, a thermal-calibration target comprising a black carton background (with $\epsilon \approx 1$) and an overlaying perforated steel-sheet (4.7 mm × 4.7 mm rectangular holes, 8 mm pitch) was produced. The latter was polished using sandpaper in order to increase its reflectivity, and consequently the contrast with the black carton background. Once the calibration target images and experimental images were both recorded, the latter were processed using an in-house algorithm developed in MATLAB. The first processing step in this algorithm seeks to identify the particles and to generate two separate frames from each raw thermal image; one containing only the particles, and a

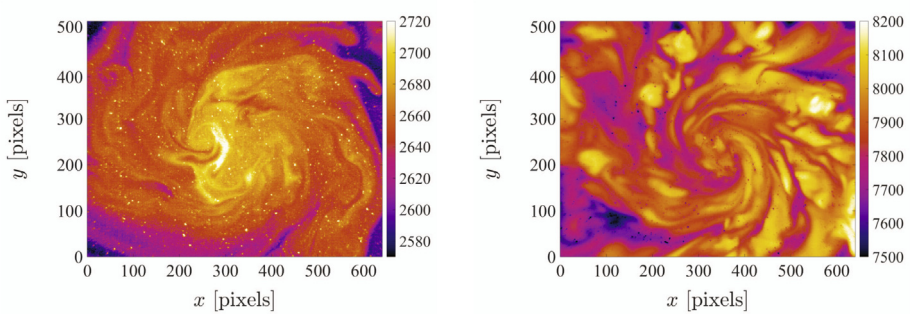

(a) Liquid temperature ≈ 10 °C. (b) Liquid temperature ≈ 50 °C.

Fig. 1. Raw IR images of heated, particle-laden flows at the air–liquid free-surface of a heated and stirred flow of water inside an open cylindrical container. Images taken with the fluid temperature being: (a) lower than the background temperature and the reflective particles appearing as localized glare spots, and (b) higher than the background temperature and the particles appearing as localized dark spots.

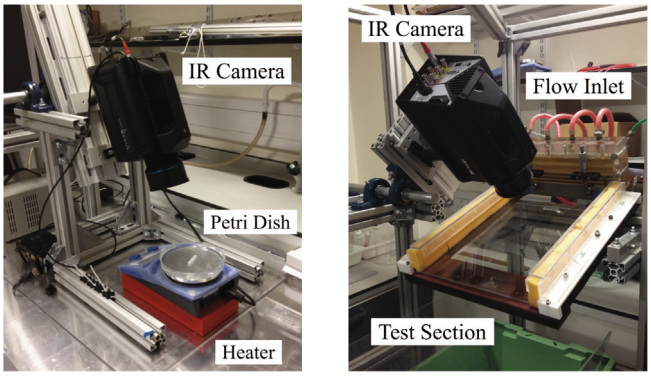

(a) Heated and stirred flow setup. (b) Film flow setup.

Fig. 2. Photographs of the experimental arrangements used: (a) for developing the experimental methodology and processing routines, and validating the IR-based temperature measurement, and (b) in the velocity validation and localized heating experiments. The images in Fig. 1 are from the arrangement in (a).

second thermal image of the liquid interface with the particles removed. In doing so, a moving-average filter with a 3×3 window is applied and subtracted from the original frame. The resulting frame is subjected to thresholding based on a (minimum) intensity level, with pixels displaying a signal intensity below the selected threshold level being set to zero. This step is used to remove any noise contained in the particle frame, thus minimizing any inaccuracies in the PIV calculation. The threshold level was determined *a priori* by conducting experiments without particles in the flow over the temperature range 20–80 °C, and applying the same moving average subtraction. The observed signals in this case originate mostly from camera noise, and can thus be used to threshold the particle detection routine. In more detail, signal probability density functions (PDFs) were generated at different mean liquid temperatures, and the signal level corresponding to 0.01 probability was plotted as a function of the mean liquid temperature. This function was then used in the particle detection routine.

Once a particle-only frame is fully processed, it is used to mask out any pixel regions corresponding to particles in the thermal frame. The thermal radiation field, which now comprises missing values in the place of particles, is reconstructed by substituting those values with the average of their neighbours. The reconstructed thermal and particle frames, along with the thermal target frame, are then imported into LaVision Davis 8.2. Mapping and optical distortion corrections for both frame sequences (thermal and particle) are performed using the target image and a pinhole model available in DaVis, with a resulting apparent resolution of 110 μm/pixel, and a root mean square (RMS) fit error of 0.4 pixels. As a final processing step, the perspective-distortion corrected thermal frames are imported back into MATLAB, and converted to 2-D temperature maps using the camera calibration curve corresponding to the employed integration-time setting. The fully corrected temperature and particle frames generated from the raw IR frame displayed in Fig. 3(a), and based on this approach, are shown in Fig. 3(b) and (c) respectively, with the colour scales optimized for illustration purposes.

Velocity-vector maps in 2-D are generated using the particle image sequence and a four-pass cross-correlation approach. A 64×64 pixel interrogation window with 50% overlap is selected for the first two passes and a 32×32 pixel window for the final two passes, resulting in a vector-to-vector spatial resolution of 1.7 mm. Further processing of the velocity maps generated during the first three passes includes application of a cross-correlation detectability filter, median filtering for removing spurious vectors, vector density filtering, interpolation/extrapolation in the empty regions, and a final smoothing step. Individual particles are also tracked (PTV calculation) using the PIV results as reference estimators of the velocity field. In this case, a $1-3$ pixel allowable particle-size range is selected, with a 4×4 pixel window for particle correlation and a ±2-pixel allowable vector range relative to the reference velocity. The PIV and PTV velocity maps obtained from the result in Fig. 3(a) are overlaid on the temperature field in Fig. 3(a) and presented in Fig. 3(d) and (e), respectively.

In addition to the experiments performed for the purpose of developing the optical technique, two more sets of experiments were conducted; an IR-based temperature validation experiment, and a velocity validation experiment. In the former, the Petri dish was filled with water (water level ≈1.5 cm) and heated to 75 °C. A 3 kΩ NTC thermistor and four fine (250 μm) K-type thermocouples were positioned to measure the temperature of a liquid volume of approximately 1 mL. Temperature measurements were recorded with the heater turned off and the water continuously stirred while cooling down, until it reached room temperature (25 °C). Using those recordings, the response of the four thermocouples was calibrated and the experiment was repeated with the thermistor removed, the thermocouples arranged equidistantly around the dish and near the air–liquid interface, and the IR camera imaging the liquid surface from above. The same image recording settings and corrections discussed earlier were implemented, and the liquid was allowed to cool to room temperature. From the IR camera recordings, the spatial standard deviation of the temperature at the air–liquid interface over the entire imaging region varied between 0.5 °C and 2.5 °C depending on the mean temperature (higher at higher mean temperatures), and therefore

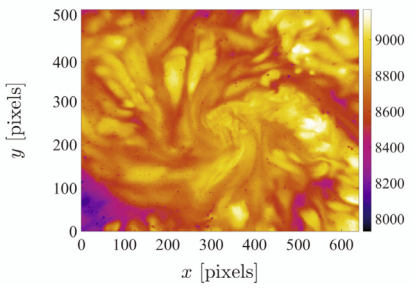

(a) Raw IR image. The colour-scale indicates the intensity of the collected signal.

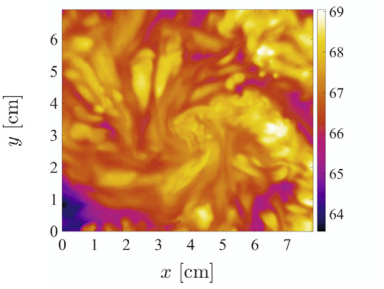

(b) Interfacial temperature measurement. The colour-scale indicates the liquid surface temperature after calibration.

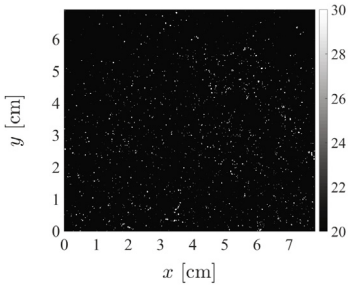

(c) Particle image. The colour-scale indicates the intensity of the particle signal following the moving average subtraction.

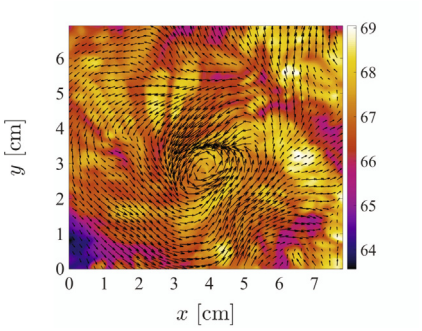

(d) Interfacial temperature and PIV measurements. The colour-scale indicates the liquid surface temperature after calibration.

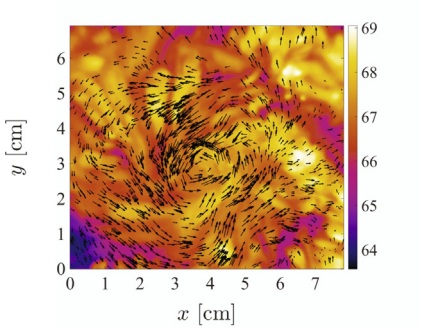

(e) Interfacial temperature and PTV measurements.

Fig. 3. (a) Raw IR image as in Fig. 1(b and c) corresponding temperature and particle frames generated during intermediate processing steps, and (d and e) combined temperature and PIV/PTV measurements at the air–liquid free-surface of a heated and stirred flow of water in an open cylindrical vessel.

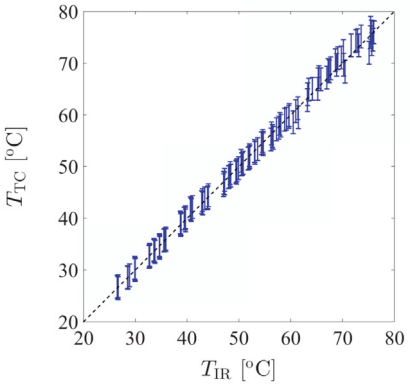

(a) Temperature measurements, T_{IR}, conducted using an IR camera, plotted against temperature measurements, T_{TC}, conducted using thermocouples, over the range 25 – 75 °C.

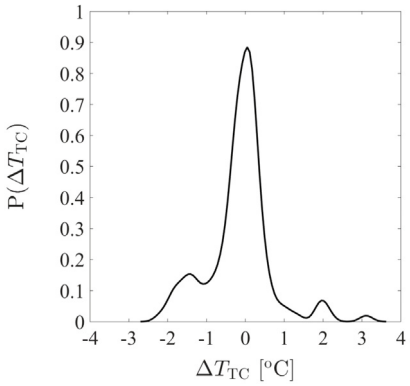

(b) PDF of the deviation between the two measurement methods, compiled using the data plotted in Fig. 3(a).

Fig. 4. Temperature validation measurements using a thermistor, thermocouples and an IR camera to image the air–liquid interface of a continuously stirred, cooling (preheated) water volume in an open container.

only a limited (1.5 cm × 1.5 cm) region of interest was considered for each thermocouple for the purposes of this test.

IR camera temperature measurements from this calibration effort (T_{IR}) are plotted against the direct thermocouple measurements (T_{TC}) in Fig. 4a PDF of the deviation between the two temperature-measurement methods (ΔT_{TC}) is plotted in Fig. 4 error bars in Fig. 4 sent the maximum measurement error associated with the thermocouples according to the manufacturer, which corresponds to 2.5 °C. The PDF plot suggests a deviation below ±0.5 °C at a confidence level of 64%, and a deviation below ±1 °C at an 80% confidence level. It should be noted that the largest deviations observed throughout the test typically originate from the initial, high temperature runs that also display the strongest (spatial) temperature inhomogeneities.

A second series of tests was conducted to assess the proposed interfacial-velocity measurement method. The setup employed in this experiment comprises a planar test-section over which liquid-film flows develop, a settling chamber installed at the

test-section inlet in order to distribute the flow evenly across the span of the substrate, and a closed flow-loop that incorporates a pump and a heat exchanger (a detailed description of the setup can be found in Refs. [31,11]). The growth of interfacial instabilities was moderated by selecting a high-viscosity liquid and a shallow inclination angle, thus allowing the film to remain flat over an extended spatial domain (distance from the inlet). In the absence of interfacial waves, an excellent approximation from the velocity profile across the liquid film can be obtained analytically using the 1-D, steady, fully developed solution of the Navier–Stokes equation for a gravity-driven flow, also referred to as the Nusselt solution. The velocity at the interface is given by:

$$U_{\mathrm{Nu}} = \frac{1}{2}\left(\frac{g\sin\beta}{\nu_{\mathrm{f}}}\right)^{1/3}\left(\frac{3Q}{w}\right)^{2/3} \tag{2}$$

where β is the inclination angle (30° to the horizontal), ν_{f} the fluid kinematic viscosity, Q the flow rate and w the film span (290 mm). The flow Reynolds number was varied in the range $Re = 0.6 - 11.8$ by adjusting the liquid flow-rate in the range $Q = 0.11\times10^{-4} - 1.28\times10^{-4}$ $\mathrm{m^3 s^{-1}}$, and the kinematic viscosity in the range $\nu_{\mathrm{f}} = 3.75\times10^{-4} - 6.42\times10^{-4}\,\mathrm{m^2 s^{-1}}$, the latter by modulating the temperature of the employed aqueous-glycerol solution (81% glycerol and 19% water by weight) between 19.3 °C and 28.3 °C. The liquid temperature was measured inside the settling chamber using a K-type thermocouple; based on this measurement and the known water/glycerol content of the solution, the liquid density and kinematic viscosity were calculated using the parametrization provided in Ref. [32]. The analytically calculated values of U_{Nu} span the range $0.05 - 0.31\ \mathrm{ms^{-1}}$.

The camera was positioned in order to image a film-flow region measuring approximately 80 mm along (240–320 mm downstream of the inlet) and 60 mm across (between the middle of the film span and towards the left wall). As the difference between the ambient and film-flow temperature never exceeded 4 °C over the course of these experiments, it was necessary to illuminate the particles in order to increase the image contrast compared to the background liquid. For this purpose, a 150 W IR heater was installed next to the test section at a distance of ≈35 cm from the imaging region. Thermocouple measurements were carried out in order to determine the effect of radiative heating on the film temperature over a range of flow rates, with the temperature difference between runs with the heater on and off amounting to 1 °C for $Re < 0.8$. On the basis of this finding, it can thus be assumed that the particular illumination method does not affect the liquid properties (or the characteristics of the flow).

The transmittance of pure glycerol in the IR portion of the spectrum was measured over the band 2.5–5 μm (the spectral range of the FLIR IR camera) using an FT-IR spectrometer (Perkin-Elmer Spectrum 100) for path lengths ranging between 60 μm and 1040 μm. Our results indicate that the penetration depth (liquid depth over which transmittance falls to $1/e$ or 37% of the incident radiative flux) corresponds to 61 μm. It can therefore be ascertained that, similar to pure-water flows, interfacial temperature measurements (over a spatially averaged depth of approximately ≈60 μm) can also be performed in flows containing glycerol. In the context of film-flow investigations this is a significant result as it allows for liquids (specifically, a wide range of aqueous-glycerol solutions) spanning a wide range of viscosities to be studied by employment of IR thermography.

The results of the velocity validation tests are presented in Fig. 5 (b), with a typical PIV map shown in Fig. 5(a). For the purpose of this experiment, only a two-pass cross-correlation was employed, with the interrogation window set to 128 × 128 pixels and the overlap set to 50%. As the measured flow-field only involves small spanwise velocity gradients, a reduced number of passes and a smaller window size allow for faster processing with a minimal accuracy penalty. From the 2-D result, only data from the region corresponding to the spanwise centreline ($x = 0$ cm in Fig. 5(a)) were considered for the velocity validation (Fig. 5(b)). These were averaged over 200 images (temporal averaging) and between 240 mm and 310 mm downstream of the flow inlet (spatial averaging). The dotted line in Fig. 5(b) corresponds to $U_{\mathrm{exp}} = U_{\mathrm{Nu}}$, while the error bars indicate the range of U_{exp} values that lie within the experimental error associated with the calculation of U_{Nu}. The extent of the error bars corresponds to average errors that arise when using the analytical expression presented in Eq. (2) to generate estimates of U_{Nu}; these are mainly attributed to the uncertainty in the value of the kinematic viscosity. The mean deviation between the experimentally derived interfacial velocity data points (U_{exp}) and the Nusselt velocity values (U_{Nu}) is ≈ 2%, with most experimental data points lying within the error bounds around the analytical estimation (≈4%).

Finally, the film-flow setup was modified in order to demonstrate the capabilities of the proposed technique in a non-isothermal film-flow experiment. The glass substrate was replaced by a perspex sheet with a 40 mm × 12 mm groove cut across the direction of the flow, at a distance of 7.5 cm from the flow inlet. A rectangular steel sleeve housing a 200 W cartridge heater was placed inside the groove, which was powered by a programmable 6 kW power supply purchased from Magna-Power Electronics Ltd. The water–glycerol solution was replaced by deionized water and cooled to 17.5 °C, the inclination angle was set to 15° to the horizontal, and the power input to the cartridge heater was set to 44 W. The sleeve temperature was first recorded as a function of the set power input without establishing a film flow, and then compared to runs with the liquid film flowing over the sleeve. Based on this comparative assessment, it was deduced that ≈8% of the applied power input is lost to the environment in the form of conductive losses to the perspex substrate and convective losses from the rear of the sleeve. Thus, for a nominal power input of 44 W, the heat flux into the liquid corresponds to ≈9.2 W cm^{-2}, whereas after accounting for heat losses, the heat flux into the liquid falls to ≈8.4 W cm^{-2}. Images were recorded downstream of the heater for flows with $Re = 80$, 100 and 120, following the procedure outlined earlier. The particle images were processed using a four-pass cross-correlation, with the final window size set to 48 × 48 pixels and the overlap to 50%. The corresponding vector-to-vector resolution was 2.64 mm. Fully-processed sample images of the temperature and velocity fields are presented in Fig. 6, revealing complex thermal features and an inhomogeneous velocity distribution. It should essentially be noted that even without the application of localized heating, 2-D waves develop upstream of the imaging location, interact and eventually break down into complex, three-dimensional (3-D) wave patterns. This suggests that the observed velocity-field non-uniformity and associated waviness is driven by inertia and gravity, rather than the thermocapillary instability, as expected for the examined film-flow conditions (Re range, liquid properties and inclination angle used here).

The combined optical technique outlined in this communication, termed ‘thermographic particle velocimetry’ (TPV), constitutes an easy to implement tool for the study of isothermal and non-isothermal interfacial flows, allowing for simultaneous spatiotemporally resolved temperature and velocity field measurements. Although the development of the TPV technique has been motivated here by the need to study gravity-driven heated liquid-film flows, the same measurement principle can be applied for the recovery of 2-D temperature- and/or velocity-field information at the interface of any multiphase flow with a sufficient density gradient between the two phases.

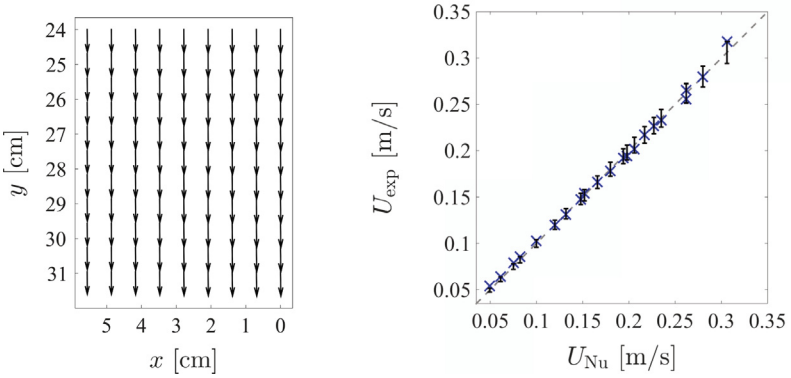

(a) Interfacial PIV measurement carried out in a flat film of Re = 11.8.

(b) Interfacial velocity measurements U_{exp} carried out using the IR camera, plotted against analytically calculated interfacial velocities U_{Nu}, for unperturbed films in the range Re = 0.6 – 11.8.

Fig. 5. Validation results for velocity measurements carried out using an IR camera at the air–liquid interface of aqueous glycerol solutions, spanning the range $U = 0.05$–0.31 ms^{-1}.

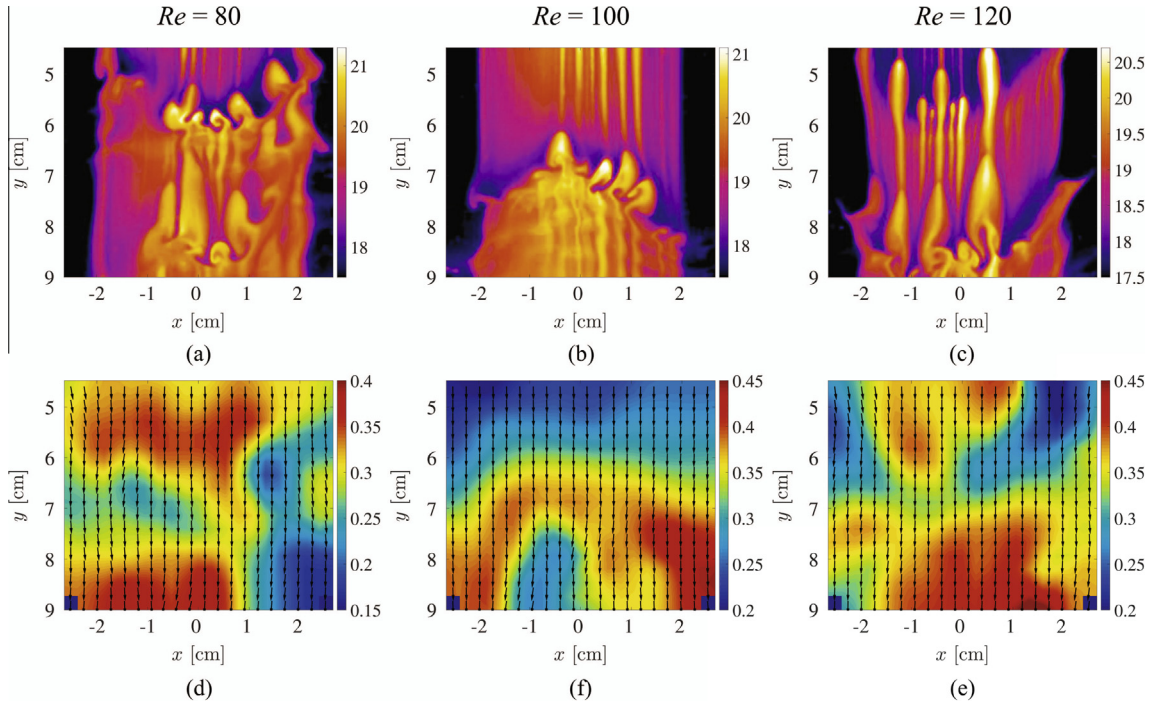

Fig. 6. Simultaneously obtained temperature-field (top) and velocity-field (bottom) measurements at the air–liquid interface of locally heated, falling water-films with Re = 80, 100 and 120. The y-axes indicate the distance of the imaging region (downstream) from the cartridge heater, the colour-scales next to the PIV maps show the magnitude of the local velocity in ms^{-1}, and the arrows indicate the direction of the flow.

A noteworthy limitation of the technique, inherently linked to the current state of IR-camera technology, is optimizing the inter-frame separation time dt between successive PIV images. Unlike typical PIV arrangements (double-pulsed laser, double-frame camera) or high-speed camera systems which allow for dt modulation independently from the recording frequency, in the case of IR cameras the recording frequency effectively determines the value of dt. Consequently, for faster flows where dt must be reduced, either a costly high-speed IR camera must be employed, or the image resolution must be reduced. Nevertheless, developments in thermography technology will continue to progressively alleviate this limitation. It is our view that the inherent simplicity and wealth of information on offer by application of the proposed technique will spearhead novel experimental investigations capable of advancing our understanding of the complex underlying physical phenomena, and the coupling between the interfacial temperature and fluid motion, in a wide range of flows.

Acknowledgments

This work was supported by the UK Engineering and Physical Sciences Research Council (EPSRC) [Grant No. EP/K008595/1]. The authors would also like to acknowledge the valuable contribution of Manish Mehta. Data supporting this publication can be obtained on request from cep-lab@imperial.ac.uk

References

[1] S. Kalliadasis, C. Ruyer-Quil, B. Scheid, M.G. Velarde, Falling liquid films, Springer Series on Applied Mathematical Sciences, 2012.
[2] P.L. Kapitza, Wave flow of thin layers of a viscous fluid, Zh. Eksp. Teor. Fiz. 18 (1948) 3–28.
[3] P.L. Kapitza, S.P. Kapitza, Wave flow on thin layers of a viscous fluid, Zh. Eksp. Teor. Fiz. 19 (1949) 105–120.
[4] S. Kalliadasis, E.A. Demekhin, C. Ruyer-Quil, M.G. Velarde, Thermocapillary instability and wave formation on a film falling down a uniformly heated plane, J. Fluid Mech. 492 (2003) 303–338.
[5] S. Kalliadasis, A. Kiyashko, E.A. Demekhin, Marangoni instability of a thin liquid film heated from below by a local heat source, J. Fluid Mech. 475 (2003) 377–408.
[6] G.M. Skotheim, U. Thiele, B. Scheid, On the instability of a falling film due to localized heating, J. Fluid Mech. 475 (2003) 1–19.
[7] W. Rohlfs, B. Scheid, Phase diagram for the onset of circulating waves and flow reversal in inclined falling films, J. Fluid Mech. 763 (2015) 322–352.
[8] S.V. Alekseenko, V.Y. Nakoryakov, B.G. Pokusaev, Wave formation on a vertical falling liquid film, American Institute of Chemical Engineers Journal 31 (9) (1985) 1446–1460.
[9] K. Moran, J. Inumaru, M. Kawaji, Instantaneous hydrodynamics of a laminar wavy liquid film, Int. J. Multiphase Flow 28 (2002) 731–755.
[10] G.M. Carlomagno, G. Cardone, Infrared thermography for convective heat transfer measurements, Exp. Fluids 49 (6) (2010) 1187–1218.
[11] C.N. Markides, R. Mathie, A. Charogiannis, An experimental study of spatiotemporally resolved heat transfer in thin liquid-film flows falling over an inclined heated foil, Int. J. Heat Mass Transfer 93 (2015) 872–888.
[12] A. Ito, N. Masunaga, K. Baba, Marangoni effects on wave structure and liquid film breakdown along a heated vertical tube, in: Advances in Multiphase Flows, Elsevier Science B.V., 1995, pp. 255–265.
[13] O.A. Kabov, I.V. Marchuk, V.M. Chupin, Thermal imaging study of the liquid film flowing on vertical surface with local heat source, Russ. J. Eng. Thermophys. 6 (2) (1996) 104–138.
[14] E.A. Chinnov, E.N. Shatskii, O.A. Kabov, Evolution of the temperature field at the three-dimensional wave front in a heated liquid film, High Temp. 50 (1) (2012) 98–105.
[15] E.A. Chinnov, O.A. Kabov, Marangoni effect on wave structure in liquid films, Microgravity Sci. Technol. 19 (3–4) (2007) 18–22.
[16] E.A. Chinnov, E.N. Shatskii, Effect of thermocapillary perturbations on the wave motion in heated falling liquid film, Tech. Phys. Lett. 36 (1) (2010) 53–56.
[17] E.A. Chinnov, S.S. Abdurakipov, Thermal entry length in falling liquid films at high Reynolds numbers, Int. J. Heat Mass Transfer 56 (2013) 775–786.
[18] F. Zhang, X. Zhao, J. Geng, Y.-T. Wu, Z.-B. Zhang, A new insight into Marangoni effect in non-isothermal falling liquid films, Exp. Therm. Fluid Sci. 31 (4) (2007) 361–365.
[19] F. Zhang, J. Peng, J. Geng, Z.-X. Wang, Z.-B. Zhang, Thermal imaging study on the surface wave of heated falling liquid films, Exp. Therm. Fluid Sci. 33 (3) (2009) 424–430.
[20] J. Peng, M.-M. Wang, J. Geng, Y.-T. Wu, Z.-B. Zhang, Falling film of ionic liquid-water binary solutions on a uniformly heated vertical wall, J. Heat Transfer 134 (1) (2012) 0145021–0145025.
[21] V.V. Lel, A. Kellermann, G. Dietze, R. Kneer, A.N. Pavlenko, Investigations of the Marangoni effect on the regular structures in heated wavy liquid films, Exp. Fluids 44 (2) (2008) 341–354.
[22] M. Rietz, W. Rohlfs, R. Kneer, B. Scheid, Investigations of the Marangoni effect on the regular structures in heated wavy liquid films, Eur. Phys. J. Spec. Top. 224 (2015) 355–368.
[23] R. Mathie, C.N. Markides, Heat transfer augmentation in unsteady conjugate thermal systems – Part I: semi-analytical 1-D framework, Int. J. Heat Mass Transfer 56 (2013) 802–818.
[24] R. Mathie, H. Nakamura, C.N. Markides, Heat transfer augmentation in unsteady conjugate thermal systems – Part II: applications, Int. J. Heat Mass Transfer 56 (2013) 819–833.
[25] O.A. Kabov, B. Scheid, I.A. Sharina, J.-C. Legros, Heat transfer and rivulet structures formation in a falling thin liquid film locally heated, Int. J. Therm. Sci. 41 (7) (2002) 664–672.
[26] R.G. Morgan, C.N. Markides, C.P. Hale, G.F. Hewitt, Horizontal liquid–liquid flow characteristics at low superficial velocities using laser-induced fluorescence, Int. J. Multiphase Flow 43 (2012) 101–117.
[27] R.G. Morgan, C.N. Markides, I. Zadrazil, G.F. Hewitt, Characteristics of horizontal liquid-liquid flows in a circular pipe using simultaneous high-speed laser-induced fluorescence and particle velocimetry, Int. J. Multiphase Flow 49 (2013) 99–118.
[28] I. Zadrazil, O.K. Matar, C.N. Markides, An experimental characterization of downwards gas–liquid annular flow by laser-induced fluorescence: Flow regimes and film statistics, Int. J. Multiphase Flow 60 (2014) 87–102.
[29] I. Zadrazil, C.N. Markides, An experimental characterization of liquid films in downwards co-current gas–liquid annular flow by particle image and tracking velocimetry, Int. J. Multiphase Flow 68 (2014) 1–12.
[30] M.Q. Brewster, Thermal Radiative Transfer and Properties, Wiley-Interscience, 1992.
[31] A. Charogiannis, J.S. An, C.N. Markides, A simultaneous planar laser-induced fluorescence, particle image velocimetry and particle tracking velocimetry technique for the investigation of thin liquid-film flows, Exp. Therm. Fluid Sci. 68 (2015) 516–536.
[32] N.-S. Cheng, Formula for the viscosity of a glycerol–water mixture, Ind. Eng. Chem. Res. 47 (9) (2015) 3285–3288.